AFRL-ML-WP-TP-2006-486

AUTOMATED SLICING FOR A MULTI-AXIS METAL DEPOSITION SYSTEM (PREPRINT)

Jianzhong Ruan, Todd E. Sparks, Ajay Panackal, Kunnayut Eiamsa-ard, F.W. Liou, Kevin Slattery, Hsin-Nan Chou, and Mary Kinsella

SEPTEMBER 2006

Approved for public release; distribution is unlimited.

STINFO COPY

MATERIALS AND MANUFACTURING DIRECTORATE
AIR FORCE RESEARCH LABORATORY
AIR FORCE MATERIEL COMMAND
WRIGHT-PATTERSON AIR FORCE BASE, OH 45433-7750

REPORT DOCUMENTATION PAGE

Form Approved
OMB No. 0704-0188

1. REPORT DATE *(DD-MM-YY)*	2. REPORT TYPE	3. DATES COVERED *(From - To)*
September 2006	Journal Article Preprint	N/A

4. TITLE AND SUBTITLE
AUTOMATED SLICING FOR A MULTI-AXIS METAL DEPOSITION SYSTEM (PREPRINT)

5a. CONTRACT NUMBER
FA8650-04-C-5704

5b. GRANT NUMBER

5c. PROGRAM ELEMENT NUMBER
78011F

6. AUTHOR(S)
Jianzhong Ruan, Todd E. Sparks, Ajay Panackal, Kunnayut Eiamsa-ard, and F.W. Liou (University of Missouri-Rolla)
Kevin Slattery and Hsin-Nan Chou (The Boeing Company)
Mary Kinsella (AFRL/MLLMP)

5d. PROJECT NUMBER
2865

5e. TASK NUMBER
25

5f. WORK UNIT NUMBER
25100000

7. PERFORMING ORGANIZATION NAME(S) AND ADDRESS(ES)
University of Missouri – Rolla
Department of Mechanical and Aerospace Engineering
B. 37 McNutt Hall
1870 Miner Circle
Rolla, MO 65409-0340

The Boeing Company
Phantom Works
St. Louis, MO

Processing Section, Metals Branch (AFRL/MLLMP)
Metals, Ceramics, and Nondestructive Evaluation Division
Materials and Manufacturing Directorate
Air Force Research Laboratory
Air Force Materiel Command
Wright-Patterson Air Force Base, OH 45433-7750

8. PERFORMING ORGANIZATION REPORT NUMBER

9. SPONSORING/MONITORING AGENCY NAME(S) AND ADDRESS(ES)
Materials and Manufacturing Directorate
Air Force Research Laboratory
Air Force Materiel Command
Wright-Patterson AFB, OH 45433-7750

10. SPONSORING/MONITORING AGENCY ACRONYM(S)
AFRL-ML-WP

11. SPONSORING/MONITORING AGENCY REPORT NUMBER(S)
AFRL-ML-WP-TP-2006-486

12. DISTRIBUTION/AVAILABILITY STATEMENT
Approved for public release; distribution is unlimited.

13. SUPPLEMENTARY NOTES
Journal article submitted to the Journal of Manufacturing Science and Engineering (Transactions of the ASME), published by the American Society of Mechanical Engineers.

PAO Case Number: AFRL/WS 06-0638, 06 Mar 2006. Report contains color.

14. ABSTRACT
A multi-axis adaptive slicing algorithm for multi-axis layered manufacturing which can generate optimal slices to achieve deposition without support structures is presented in this paper. Different from current adaptive slicing, this technique varies not only layer thickness but also in slicing/building direction. Aware of potential problems of previous research on slicing, the work in this paper focuses on innovative geometry reasoning and analysis tool-centroidal axis. Similar to medial axis, it contains geometry and topological information but is significantly computationally cheaper. Using a centroidal axis as a guide, the multi-axis slicing procedure is able to generate a "3-D" layer or change slicing direction as needed automatically to build the part with better surface quality. This paper presents various examples to demonstrate the feasibility and advantages of centroidal axis and its usage in the multi-axis slicing process.

15. SUBJECT TERMS
CAD/CAM, Layered manufacturing, Multi-axis slicing, Geometry reasoning

16. SECURITY CLASSIFICATION OF:			17. LIMITATION OF ABSTRACT:	18. NUMBER OF PAGES	19a. NAME OF RESPONSIBLE PERSON (Monitor)
a. REPORT	b. ABSTRACT	c. THIS PAGE			Mary Kinsella
Unclassified	Unclassified	Unclassified	SAR	36	19b. TELEPHONE NUMBER *(Include Area Code)* N/A

Standard Form 298 (Rev. 8-98)
Prescribed by ANSI Std. Z39-18

AUTOMATED SLICING FOR A MULTI-AXIS METAL DEPOSITION SYSTEM

Jianzhong Ruan, Todd E. Sparks, Ajay Panackal, Kunnayut Eiamsa-ard, and F. W. Liou*
Department of Mechanical and Aerospace Engineering
University of Missouri – Rolla

Kevin Slattery and Hsin-Nan Chou
Phantom Works
The Boeing Company, St. Louis

Mary Kinsella
Air Force Research Laboratory
Wright-Patterson AFB

ABSTRACT

A multi-axis adaptive slicing algorithm for multi-axis layered manufacturing which can generate optimal slices to achieve deposition without support structures is presented in this paper. Different from current adaptive slicing, this technique varies not only layer thickness but also in slicing/building direction. Aware of potential problems of previous research on slicing, the work in this paper focuses on innovative geometry reasoning and analysis tool-centroidal axis. Similar to medial axis, it contains geometry and topological information but is significantly computationally cheaper. Using a centroidal axis as a guide, the multi-axis slicing procedure is able to generate a "3-D" layer or change slicing direction as needed automatically to build the part with better surface quality. This paper presents various examples to demonstrate the feasibility and advantages of centroidal axis and its usage in the multi-axis slicing process.

Keyword: CAD/CAM, Layered manufacturing, Multi-axis slicing, Geometry reasoning

1. INTRODUCTION

Since its appearance in the mid 80s, Layered Manufacturing (LM) technology has attempted to provide an efficient approach to build parts directly from a CAD model [e.g., 1-5]. Most of the current RP systems are built on a 2.5-D platform. Among them, the laser-based deposition process is a potential technique that can produce fully functional parts directly from a CAD system and eliminate the need for an intermediate step.

* Address all correspondence to this author: liou@umr.edu; 573-341-4603

However, such a process is currently limited by the need for supporting structures – a technology commonly used in all the current RP systems. Support structures are not desirable for high strength and high temperature materials such as metals and ceramics since these support structures are very difficult to move. As a result, the current laser deposition process, such as LENS (Laser Engineering Net Shaping [6]) from Optomec Inc., can only build fully dense metal with relatively simple geometry [7,8]. Therefore, building parts with complicated shapes becomes a hurdle for the process due to limited motion capability.

In order to expand the applications of metal deposition processes, multi-axis capability is greatly needed. A multi-axis rapid manufacturing system can be created/constructed by adding extra degrees of mobility to a deposition system or by mounting a laser deposition device on a robot arm. The configuration could also be a hybrid system in which a metal deposition system is mounted on a four or more axes CNC machine. With the addition of extra rotations, the support structures may not be necessary for the deposition process in order to build a complicated shape. Figure 2 illustrates the process to build an overhang structure on a 2.5D and multi-axis deposition system. Due to the nature of the deposition process, it is driven by a so-called "slicing" procedure, which uses a set of parallel planes to cut the object to obtain a series of slicing layers. Most of the research is focused on 2.5D slicing in which the building/slicing direction is kept unchanged (usually Z+ direction) and lacks the capability of changing directions to fully explore the capability of multiple degrees of freedom. Few researchers have addressed issues on multi-axis slicing. However, each algorithm has its own drawbacks which will be discussed in the next section.

A solution to this problem is to change the slicing/building direction as needed, which could eliminate or significantly decrease the usage of a support structure to build overhangs or complicated shapes. This paper introduces a new slicing algorithm based on centroidal axis computation. The method not only presents a computationally cheap geometry extractor but also overcomes the problems experienced by other multi-axis slicing procedures. This paper is organized as follows: In section 2, 2.5D slicing methods and some research on multi-axis slicing are summarized; then the research problem for this paper is defined and analyzed. The computation of centroidal axis of an object is

discussed in section 3. The multi-axis slicing procedures are presented in the next section. Some examples are shown and a discussion is presented in section 5. The paper is concluded in section 6.

2. Related Work

2.1 Literature review

In LM processes, slicing is the process that is represented as a set of layers formed by "slicing" a CAD model with a set of horizontal planes [9]. The distance between planes is called "layer thickness". Differences in quality can be achieved by controlling the layer thickness. Research on 2.5-D slicing procedures and deposition toolpath for layered manufacturing processes has been widely conducted. Dolenc and Makela [10] introduced cusp height to control the tolerance. Since then, various efficient and reliable processes for 2.5-D slicing procedures have been studied based on controlling cusp height and meeting the critical surfaces [11-14]. However, the geometric error may occur when the angle between surface normal and the slicing direction is close to 90°. To solve this problem, some researchers presented a slicing method using volume difference between adjacent slicing layers [15, 16]. Rather than computing the cusp height, this method determines layer thickness by comparing the area difference between two neighboring layers after conducting Boolean operations. To some extent, these methods help to improve the efficiency and quality for the deposition system; however, not all of these methods adopt multi-axis into the slicing algorithm; thus, they lack the ability to handle a more complicated multi-axis layered manufacturing process.

Recently, some research has been focused on multi-axis slicing to drive a multi-axis deposition system in order to deliver a more efficient manufacturing system. The projection method is reported to be used to find the new building direction for overhang structure [17]. In this work, the part is decomposed according to the projected information. The building direction is determined from a building map constructed for a decomposed component. However, in some cases, the building direction does not match the surface normal, which leads to a greater staircase effect. Furthermore, a collision may occur which is difficult to avoid. Figure 3 shows an example to illustrate this situation.

A thin/transition wall can be used to build overhang structures on the platform of the multi-axis deposition process. In this method, the building/slicing direction of one

slice is determined by the previous layer. To build an overhang structure, the machine is turned 90º to start depositing a transition, named thin wall. After the wall is finished, the part is flipped back to its original direction to continue the deposition process. In this method, 3-D slicing is used to generate non-uniform thickness layers to slice the curve (freeform) surface. However, transition/thin wall usage is limited by physical capability and its results cannot always be realized in the deposition system [18, 19]. In some cases, the rotated deposition is impossible to implement, as shown in Figure 4. The slicing methods and their drawbacks are summarized in Table 1.

The projection and thin wall method complement each other very well. It will benefit the multi-axis deposition process significantly to integrate projection and 3-D slicing together. The obstacle is an automatic determination on how to apply different slicing methods; in other words, the challenge is to understand geometry and use the information to automatically apply the different slicing strategies. Therefore, finding a suitable geometry extractor/recognizing tool is very critical for a multi-axis slicing method.

Medial axis, also referred to as skeleton, has been introduced to study biological shapes for a long time [20]. Medial axis represents 3-D shapes with a series of curves/points, like the skeleton of the human body. This concept has been widely used in pattern recognition, shape analysis, and mesh generation [21-24]. Various methods have been studied to find 3-D medial axes [25, 26]. Figure 5 shows the medial axes of a bunny, and it provides us with an easy tool to understand the geometric structure of complex shapes. The benefit of the medial axis is that it provides global and local topological information of a 3-D shape with a simple structure. Since medial axis brings sufficient information (topological and geometric), it is prudent to use medial axis for process planning in order to find optimal results. However, finding medial axis is very computationally expensive. To compute skeletons of geometry shown in Figure 5, more than 200 seconds (in 2000 PC Windows environment) are needed. A more efficient geometry information extraction method is urgently needed in order to lead to an intelligent multi-axis slicing method.

2.2 Problem definition

As mentioned above, the research reported in this paper is to find an intelligent, robust slicing algorithm for the multi-axis deposition system. The problem is defined below

Given (Geometry *G*)

Output Collision-free slicing for a multi-axis deposition system.

The algorithm is able to automatically determine the slicing strategy with extracted geometric information. Thus, developing a geometry information extraction tool is very important in the slicing process. Finding medial axis is very time consuming and the result cannot be used to determine the slicing process directly. Furthermore, redundant information may be misleading and is difficult to process. However, the skeleton-like information is still very useful in the slicing process. Therefore, the first objective of this research is to develop a method which is computationally efficient and provides "skeleton" information of an object. Instead of searching points with equal distance to the surrounding surfaces to form medial axis, the centroids of the part on different locations are obtained to form a centroidal axis.

Once the centroidal axis is extracted, the geometry information, including topological information of the part can be obtained. This information will be analyzed to guide the multi-axis slicing process in order to make it more efficient. The key task in this research is defined below:

1. Centroidal axis computation and formation
2. Collision-free multi-axis slicing procedure based on centrodial axis

3. Centroidal Axis Computation

The computation of the centroidal axis including the definition of the centroidal axis, the computation analysis and the algorithm to extract centroidal axis is discussed in this section.

3.1 Definition

Usually, for a 2-D shape, the medial axis is composed of points with equal distance to the neighboring edges (boundary). The entire search is a trial and error process which is very time consuming. The computation to find the medial axis for a 3-D shape costs more time. To obtain an efficient geometry analysis tool, the centrodial axis is defined in this research to extract the topological and geometrical information in the

multi-axis slicing process. Similar to medial axis, centroidal axis is also composed of a series of points which are centroids of cross sections at different locations. A cross section is the intersecting result of a planar surface and an object. A planar surface can be defined by a position and a normal direction. At a particular position, there are infinite directions. Therefore, there are infinite cross sections, which may yield infinite centroidal axes for the object. Figure 6 illustrates this situation by showing three different centroidal axes along different directions for a simple block. To simplify the situation, three major directions in the Cartesian coordinate system are selected as candidate directions to compute centroids. Therefore, the centroidal axis is no more than an aggregation of nodes which is composed of a geometric position and links connecting the node to other nodes. It can be expressed as

$$A = \{P_1, E_{11}...E_{1k} \mid ... \mid P_i, E_{i1}...E_{ik} \mid ... \mid P_n, E_{n1}...E_{nk}\} \quad i = 1....n$$

$$E_{il} =< P_i, P_l > \quad i \neq l \qquad (1)$$

where P_i is the centroid of a cross section and E_{il} is the link connecting P_i and P_l. It should be noted that each outer loop in a cross section defines an independent centriod. The centroidal axis along {0,0,1} of the block shown in Figure 6 can be expressed as below

$$A = \{P_1(0,0,0.01), \phi \mid ... \mid P_7(0,0,1), E_7 < P_{6,} P_7 >\}$$

According to this definition, the position of the centroid can be obtained by computing the geometry center of a cross section; the linking edge can also be determined by the relationship between two centroids, which is defined by two associated cross sections. Thus, the topological relationship between two centroids is actually formed by the corresponding cross sections. In this definition, the centroidal axis not only contains the geometric information by locating the various center positions of different cross sections but also directly gives the topological information by forming the directed link between centroids. Furthermore, computation of the geometric center for a cross section takes much less time than to find a point along the medial axis in a 3-D space. Therefore, the centroidal axis is a very efficient tool to define geometry and topology of an object and it can be used to guide the multi-axis slicing process.

3.2 Computation analysis

To compute the centroidal axis is to find the centroid of different cross sections. Due to the nature of the deposition process, the initial building direction is always upward (Z up direction $\{0,0,1\}$); therefore it is reasonable to use this direction as the initial normal direction for the planar surface to obtain the first cross section. However, without changing the direction, the yielded centroid may not be desirable. Figure 7a shows an "L" shaped block. If the normal direction of the intersecting plane is kept as "Z" up, all centroids generated are shown in Figure 7b. Connecting the adjacent centroids yields an axis. It is obvious that this centroidal axis does not contain the "desirable" centroids as the top portion of the "L" in Figure 7 (a) will need to be built with overhang. It may be more desirable if the top centroids are along vector $\bar{L}$ in Figure 7(c) as this suggests that the machine will turn 90 degrees to build the top portion of the "L" block.

3.2.1Determination of normal direction of intersecting plane

In order to obtain a proper centroidal axis, the normal direction of the intersecting plane may be changed as needed; in other words, the objective is to select a cross section among the possible candidates to extract the geometric center at a particular location. Only considering the external boundary of a cross section, the relationship between two adjacent cross sections can be defined by applying the Boolean operation after projecting the upper slice to the lower slice. Let A_{lower} and A_{upper} denote the area of external contour of two adjacent cross sections (lower cross section and upper cross section, respectively). After projecting the upper slice to the lower slice, the conducting operation $A_{upper} - (A_{lower} \bigcap A_{upper})$ yields the result listed below and Eq. 2.

- If the result is A_{upper}, it indicates that upper cross section does not intersect with the lower cross section. Assuming the distance between two cross sections is small, this implies that the geometry is broken and the current centroidal axis search ends (Fig. 8a).
- If the result is ϕ, it indicates that upper cross section is smaller than the lower cross section, which indicates that the geometry continuity is maintained and centrodial axis searching is continued with the same normal direction for the intersecting plane (Fig. 8b).

- If the result is composed of various areas (Fig. 8c), the geometry center position of each area should be checked to identify the geometry continuity break. It usually occurs when the distance between a geometry center and the lower cross section is much greater than the distance between the upper and lower cross section. It indicates a change of normal direction for the next intersecting plane.

$$A_{upper} - (A_{upper} \cap A_{lower}) = \begin{cases} A_{upper} \\ \phi \\ \Delta A_1, \Delta A_2, ..., \Delta A_n ; \sum_{k=1}^{n} \Delta A_k < A_{upper} \end{cases} \quad (2)$$

The new normal direction is dependent on the relative position of the geometric center (G_t) of each identified area and the centroid (C_i) of the lower cross section. Since the normal direction only follows one of the three axes, the new direction is selected based on the minimum angle criteria described below:

Let $\overrightarrow{P_t}$ denote the vector formed by G_t and C_i, then the next normal direction is one of the candidate directions (both directions along each major axis X, Y, Z) which forms a minimum angle with $\overrightarrow{P_t}$, as illustrated in Figure 7c.

3.3.2 Determination of intersecting location

Let S_{low}, $\overrightarrow{P_{low}}$ denote the intersecting location and normal direction of the current cross section. The tentative intersecting location can be expressed as

$$S_{next} = S_{low} + \overrightarrow{P_{low}} \bullet inc \quad (3)$$

where inc is the increment resolution, a predefined value.

In this research, inc is defined as the minimum distance between two non intersecting surfaces of an object. Once the new cross section (the upper one) is obtained, apply Eq. 2 on the lower and upper cross sections. If no change in normal direction is found, the S_{upper} can be used in the next step to search for the centroidal axis. If the normal direction needs to be changed, the lower cross section is used to find the new direction. Let G denote the geometric center of the area identified by using Eq. 2. Let $\partial Lower$, C_{lower} denote the external boundary and the centroid of the lower cross section respectively.

Let $\vec{P}$ denote the new normal direction. Projecting $\partial Lower$ along $\vec{P}$ yields a maximum value T, and the new intersecting S_{next} location can be expressed as

$$S_{next} = C_{lower} + (T - \overrightarrow{(C_{lower} - O)} \bullet \vec{P} + \varepsilon) \bullet \vec{P}) \qquad (4)$$

while O is the origin point and ε is variable to avoid floating error. In this research, ε =0.001

3.2.3 Topology identification

In most cases, connecting the centroids of the upper cross section and lower cross section forms the linking edge. When the normal direction is changed, the link edge cannot be obtained by directly connecting the centroids since the topological relationship is lost for two cross sections. Figure 8a illustrates this case. During the searching process, each normal direction change can be regarded as a new "branch" which is generated. By tracking the searching status, the "branch" can be connected to its corresponding centroid. Figure 8b demonstrates this process.

All links to connect centroids form vectors. If the direction given by the vectors does change significantly, it indicates a C^1 break. By checking the angle between two adjacent links, all these "break" links can be found. The "break" links are marked in blue in Figure 9b. In addition, the connecting links store the topological relationship among all centroids. In this relationship, if a centroid *E* has another centroid *Ex* connected to it, *E* is called *Ex*'s father and *Ex* is *E*'s child; all other centroids connected to *E* are *Ex*'s brothers. The same concept is applied on the link as well.

3.2.4 Algorithm summary

The algorithm to extract the centroidal axis is summarized below. Assuming that the part is placed on the XOY plane, the initial intersecting point is *P* (0,0,0+ε) and the initial normal direction is $\vec{L}$ {0,0,1}. Given Part *B*, increment step *t*, distance threshold *d*, small amount variable ε, the procedure stops when no more cross sections are obtained. The algorithm is listed in Figure 9.

The entire searching process is a recursive one. When the normal direction change is identified, a new searching process is triggered. The steps *Bs* ← *GetSweepBody* and *B* = *B-Bs* are used to allow the geometry to be checked only once. In the process of

command *GetSweepBody*, different cross sections of the extracted centroidal axis are used to form a sweeping body to represent the portion of geometry in which centroidal axes are already found. Since the axis searching process is a branch-first one, operation of *B = B-Bs* eliminates the geometry which has been checked. *FindConnectingLink* is to connect the "child branch" centroidal axis back to the main "branch" by the distance from the first centroid in the "child branch". The function of *CrossSectionAnalysis* is to analyze the cross section and make a decision based on the discussion. The entire searching process stops until all branch/local search processes are finished.

3.2.4 Summary

The centroidal axis is much simpler than the medial axis searching process. Since most of the computation is conducted on a 2-D domain (a planar cross section), it does not require the complicated trial and error tracking techniques used in a 3-D medial axis searching process. Furthermore, it provides geometry information as well as topological information which are very helpful for the multi-axis slicing process. Its characters are summarized below.

- The simplicity of the centroidal axis makes the geometry analysis process easier.
- The centroidal axis provides a global perspective on the geometry to be deposited, which allows the slicing procedure to be conducted on an optimal sequence.

Figures 10 and 11 show two examples respectively. In Figure 10, the centroidal axis of a pen rack is shown. It reflects the geometry change by following the inclined rack shape. The centroidal axis illustrated in Figure 11 demonstrates the topological information contained in it. The two curved branches are associated with the two separate centroidal axes which are connected to a common centroid. The entire centroidal axis is put in an adjacent graph which is used later to determine the slicing sequence.

4. Multi-Axis Slicing

In this section, the algorithm of multi-axis slicing based on the centroidal axis is discussed. The multi-axis slicing process starts with analyzing the topological information from the centroidal axis; then the decomposition operation is conducted according to the adjacent graph. For each subcomponent obtained from decomposition, the multi-axis slicing is performed. Finally, the collision free slicing sequence is generated. In addition, the cutting plane to generate the slicing layer is not parallel to

each other, which may result in a non-uniform layer [18] or "3-D" layer. Recently, a non-uniform layer was achieved by using the hybrid manufacturing system [27]. Usually, for metal cladding/deposition system, energy level (laser power density), powder feeding rate, scanning speed, and gas pressures are major parameters to decide the final result, like layer height/thickness. By varying parameters during the cladding process, the thickness can be changed [28]. Another way to build a "3-D" layer is by using several very "thin" layers of a different profile to form a relatively "thick" "3-D" layer. The "3-D" layer technique is adopted in this research to keep the geometry continuity and obtain a better deposition quality. Figure 12 illustrates the difference between a "3-D" layer and a regular slicing layer.

4.1 Decomposition using centroidal axis

This task is to decompose the part into sub-components according to the centroidal axis. Since the slicing process follows the extracted centroidal axis, usually each "break" link indicates a C^1 discontinuity or rapid change in geometry. Decomposing the part finds the splitting surface which can be used to separate the geometry. In a word, the appearance of a splitting surface implies a C^1 discontinuity or rapid change in geometry. It can be a planar surface, or a non-planar parametric surface. In some cases, there are no surfaces which exist for splitting.

Let $\vec{L}$ and $\overrightarrow{L_{pre}}$ denote the unit vector formed by a "break" link and its "father" link. From observation, for a planar splitting surface, the angle between its normal direction and $\overrightarrow{L_{pre}}$ should be very small; in this research, the value is set to 10^o; since the centroidal axis changes direction significantly, splitting surfaces have concave edges on their boundary. The $\vec{L}$ may intersect with the splitting planar surface. However, in most cases, $\vec{L}$ is inside the body. Therefore, the splitting planar surface does not always intersect with $\vec{L}$. In this situation, the projection checking method is conducted. For each planar surface, projecting its external boundary along $\vec{L}$ yields a maximum and a minimum value (denoted as $Proj_{max}$ and $Proj_{min}$). If the planar surface is a splitting surface for the "break" link $\vec{L}$, it should meet the criteria below:

$\overrightarrow{(Pos_{start} - O)} \bullet \vec{L} \le Proj_{max} \le \overrightarrow{(Pos_{end} - O)} \bullet \vec{L}$ or

$$\overrightarrow{(Pos_{start} - O)} \bullet \vec{L} \leq Proj_{min} \leq \overrightarrow{(Pos_{end} - O)} \bullet \vec{L} \quad (5)$$

where Pos_{start}, Pos_{end} is the starting and ending position of centroids defining the vector $\vec{L}$ and O is the origin of coordinate system.

Therefore, the three criteria to identify the planar splitting surface are listed below:

1.Angle between unit vector formed by "break" link and normal is less than 10^o.

2.The boundary of the surface contains a concave edge.

3.The projection requirement is met.

Once a splitting surface is identified, the given object can be decomposed as two bodies. The body containing Pos_{end} is the children of the other, which still follows the topological relationship defined in the centroidal axis. In the deposition procedure, if a splitting planar surface cannot be identified, the silhouette edges method reported in [17] is applied here to decompose the part. The result of the deposition is a topological tree in which each node represents a sub-component and the edge defines the "father-child" relationship.

4.2 Slicing procedure

In a regular 2.5 deposition system, the building direction is always kept as Z up without change. The only variable in the slicing procedure is the layer thickness or slicing step. However, in the multi-axis slicing procedure, not only the layer thickness can be changed but also the slicing/building direction can be changed. Thus, the task in this procedure is to find the slicing location and direction within the given error limit. With the change of slicing direction, the support structure required in the 2.5D layer deposition system to build overhang structures can be saved.

4.2.1 Initial slicing position and direction

For each sub-component B obtained from the decomposition, the initial slicing direction is always reverse to the normal direction of the base surface. Let $\overrightarrow{D_{slicing}}$ and P_{in} denote the slicing direction and any point on the boundary of base surface, then the initial slicing position can be expressed as:

$$P_{slicing} = P_{in} + \overrightarrow{D_{slicing}} \bullet \Delta \quad (6)$$

where Δ is the small value

The initial slicing plane formed by this slicing position and direction intersects with the body to yield the first slice. In addition, it intersects with the centroidal axis to obtain the initial slicing position on the centroidal axis.

4.2.2 Slicing direction and position selection

As a deposition process, the essential is to be able to deposit an object with the fastest speed and best quality. Controlling the quality reduces the "staircase" effect in the deposition process. Since limiting the volumetric difference between layers results in a better performance than the cusp height controlling method [Yang03], the concept is adopted in this research to improve the slicing quality. As mentioned before, the slicing strategy used in this research may yield a "3-D" layer, in which the points on the upper slice have a different distance to the lower slice; therefore computing a method to find the volumetric difference needs to be redefined [29].

There are physical limitations on the maximum layer thickness that can be formed by a deposition machine, denoted as ΔL_{max}; let *VolDiff* denote as the volumetric difference. In a deposition layer, the maximum deposited thickness cannot go beyond this limit. Furthermore, there is also a limit on volumetric difference; thus, two constraints are obtained for the slicing procedure

$$\begin{aligned} \Delta L_{slicing} &\le \Delta L_{\max} \\ VolDiff &\le VolDiff_{pre} \\ \Delta L_{slicing} &\ge \Delta L_{\min} \end{aligned} \qquad (9)$$

where $VolDiff_{pre}$ is a predefined value for maximum volumetric difference and $\Delta L_{\max}$ is the maximum layer thickness for a slicing layer, $\Delta L_{\min}$ is the minimum layer thickness for a slicing layer,

With given slicing step Δ, found slicing direction $\overrightarrow{D_{lower}}$ for previous layer and slicing position P_{lower} on the centroidal axis, the optimal objective is to find a slicing position and direction for the next slice to meet the criteria defined in Eq. 9. The tentative slicing position for the next slice can be found by a point P_{upper} on the centroidal axis with a distance Δ to P_{lower}, then the tentative slicing direction $\overrightarrow{D_{upper}}$ will be found by checking the associated link in the centroidal axis; thus with P_{upper} and $\overrightarrow{D_{upper}}$, a guided slice is obtained.

If Eq 9 is satisfied, then the slicing procedure continues until no slice is found; otherwise, the following steps are conducted.

1. $\overrightarrow{D_{upper}} = (\overrightarrow{D_{upper}} + \overrightarrow{D_{lower}})/2$
2. Getting a slice at P_{upper}, step 1 is repeated until Eq.(9) is satisfied or the angle between $\overrightarrow{D_{upper}}$ and $\overrightarrow{D_{lower}}$ is less than a small value ε then go to step 3.
3. $\Delta_{new} = \Delta - \Delta/4$ then find a new tentative slicing position and direction repeating step 1, 2 until Eq. 9 is satisfied.

4.2.3 Slicing sequence

Using the topological relationship after deposition, a general slicing sequence can be found. Similar to the sequence presented in [Singh01], a "child" sub-component cannot be built until its father has been deposited. However, when a child has "brothers", the collision is considered in determining the building/slicing sequence. Usually, a deposition nozzle includes a tip and body which are defined as a cone and cylinder respectively. If the deposited part is B_{dep}, then Eq 10 is satisfied if no collision occurs

$$(B_{dep} \bigcap B_{tip} \bigcap B_{body}) = \phi \qquad (10)$$

where B_{tip} is the representation of the tip and B_{body} is the body of the nozzle.

The deposited body can be obtained by sweeping the slicing layer to form the geometry. When a collision occurs, the slicing procedure switches between a sub-component and its brothers. In other words, several sub-components are built simultaneously. In order to shorten the traveling time of the deposition nozzle between different sub-components, the deposition of each sub-component is discontinued just before a collision happens.

4.3 Algorithm summary

The entire multi-axis algorithm is developed based on the centroidal axis extraction. The trial and error method has been adopted to determine the slicing location and direction to meet the volumetric difference requirement. The final result is a slicing sequence defined as a slicing contour queue. Given Part *B*, maximum layer thickness ΔL_{max}, minimum layer thickness ΔL_{min}, allowed volumetric different *v*, the algorithm is listed in Figure 13.

5. Example and Discussion

The presented algorithm has been implemented in VC++ using an ACIS geometry kernel. Figure 14 shows the slicing result of the examples shown in Figure 11. In Figure 14, the example demonstrates the "3-D" layer in the C^1 continuous non-planar branch slicing procedure. The slicing direction is kept changed to reflect the direction change in the centroidal axis. This matches the geometry shape in two curved branches. Furthermore, using the centroidal axis, the "critical plane" [16] in the deposition process is detected easily with a "break" link in the centroidal axis.

Another hinge example and its deposition result are shown in Figure 15. The part is decomposed into five subcomponents (1,2,3,4,5) as shown in Figure 15(c). The slicing result is shown in Figure 15(d). The deposition starts from building the subcomponent 1 then the subcomponent 2, 3 are built after rotating the part 90º around X axis. The subcomponents 4, 5 are finished after rotating the part 180º around Y axis.

All examples have illustrated the usage of the centroidal axis and the "3-D" layer in multi-axis. The computation time of the centroidal axis for three examples is about 2, 3, 3 seconds respectively on a P4 (2.8 GHz) PC; therefore, it can be safely concluded that the centroidal axis has more of an advantage than the medial axis in terms of the usage in the multi-axis slicing process. It contains geometric and topological information which can be used to guide the entire slicing procedure.

Although the deposition follows the process planning very well, some very small features may be missed due to the physical limitation like minimum track width. The powder used in the deposition experiment is 4140. The author also experimented with different materials like H13 tool steel to build the part. Following the same slicing and scanning toolpath result, there is a geometric difference between the deposition results due to different properties of the material. The knowledge of material could be integrated into process planning.

6. Conclusion

The multi-axis deposition system can potentially make solid freeform fabrication very attractive to industry. This paper presents the slicing of CAD models based on the centroidal axis for such machines. The usage of the centroidal axis in multi-axis slicing provides the following advantages:

1.The centroidal axis is very computationally cheap.

2.Combined precise geometry and topological information in a very simple format.

3.It can be used directly to guide the multi-axis slicing procedure.

An algorithm to extract the centroidal axis is discussed in this paper. By using the centroidal axis, the multi-axis slicing process integrates the concepts of the "3-D" layer and decomposition of an object to make the slicing result accurate. The entire process is automatically driven by the centroidal axis without human interference. The algorithm is implemented on a geometry kernel, therefore it is very easy to extend its application on any geometry format including STL.

On the other hand, the implemented method still has its own limitations. Illustrated in Figure 16, the centroidal axis of the shape does not indicate the change of the geometry and the deposition will fail without support structure. Rapid geometric changes can be detected by comparing the adjacent slicing layers. This problem could be solved by decomposing the upper part into several sub-components. In addition, as discussed before, the material should be considered and processed in the process planning. Future work on this topic will be focused on these challenges.

Acknowledgements

This research was supported by the National Science Foundation Grant Number DMI-9871185, U.S. Air Force Research Laboratory contract # FA8650-04-C-5704, and UMR Intelligent Systems Center. Their support is greatly appreciated.

Reference:

1] Das, Suman; Harlan, Nicole; Beaman, Joseph and David Bourell, "Selective Laser Sintering of High Performance High Temperature Metals", *Proceedings of Solid Freeform Fabrication*, Austin, TX, 1996, pp 89-96.

[2] Fodran, Eric; Koch, Martin and Menon, Unny, "Mechanical and Dimensional Characteristics of Fused Deposition Modeling Build Styles", Solid Freeform Fabrication Proceedings, 1996, pp 419-442.

[3] Jacobs, P. F.," Stereolithography and Other RP&M Technologies: From Rapid Prototyping to Rapid Tooling" *Society of Manufacturing Engineers*, 1995.

[4] McAlea, Kevin and Hejmadi, Uday," Selective Laser Sintering of Metal Molds: The RapidTool (TM) Process", Solid Freeform Fabrication Proceedings, 1996, pp 97-104.
[5] Pope, Matthew J.; Patterson, Mark C.L. Patterson; Zimbeck, Walter and Fehrenbacher, Mark, "Laminated Object Manufacturing of Si3N4 with Enhanced Properties", Solid Freeform Fabrication Proceedings, 1997, p 529-536.
[6] Hofmeister, W., M. Griffith, M. Ensz, J. Smugeresky, Solidification in Direct Metal Deposition by LENS Processing, JOM-Journal Of The Minerals Metals & Materials Society, v. 53(#9) pp. 30-34 Sep 2001.
[7] Laeng, J.; Stewart, J.G.; and Liou, F.W., "Laser Metal Forming Processes And The Application In Rapid Prototyping of Metallic Parts", Proceedings of the 2nd International Conference on Advanced Manufacturing Technology, Johor Bahru, Malaysia, August 2000a.
[8] Laeng, J.; Stewart J.G.; and Liou, F.W., "Laser Metal Forming Processes for Rapid Prototyping – A Review," International Journal of Production Research, Vol.38, No.16, pp.3973, 2000b.
[9] Pandey, Pulak Mohan; Reddy, N. Venkata and Dhande, Sanjay G., "Slicing procedures in layered manufacturing: a review", *Rapid Prototyping Journal*, Vol. 9 No. 5 2003, pp.274-288.
[10] Dolenc, A and Mäkelä, I, "Slicing procedures for layered manufacturing techniques", *CAD*, Vol. 26, Feb. 1994, pp.119-126.
[11] Kulkarni, Prashant and Dutta, Debasish, "An accurate slicing procedure for layered manufacturing", *CAD*, Vol.28, No.9, 1999, pp.683-397.
[12] Kumar, Madhup and Choudhury, A. Roy, "Adaptive slicing with cubic path approximation", *Rapid Prototyping*, Vol. 8. No. 4, 2002, pp.224-232.
[13] Ma, Weiyin and He, Peiren, "An adaptive slicing and selective hatching strategy for layered manufacturing", *Journal of Material Processing Technology*, 1999, pp.191-197.
[14] Tata, Kamesh; Fadel, Georges; Bagchi, Amit and Aziz, Nadim, "Efficient slicing for layered manufacturing", *Rapid Prototyping*, Vol. 4. No. 4, 1998, pp.151-167.
[15] Luo, Ren C.; Chang, Yi Cheng and Tzou, Jyh Hwa, "The development of a new adaptive slicing algorithm for layered manufacturing system", *Proceedings of the 2001 IEEE International Conference on Robotics & Automation*, Seoul, Korea, May 21-26, 2001.
[16] Yang, Y.; Fuh, J.Y.H.; Loh, H. T. and Wong, Y. S., "A volumetric difference-based adaptive slicing and deposition method for layered manufacturing", *Journal of Manufacturing and Science*, Vol.125, Aug. 2003, pp.586-594.
[17] Singh, Prabhjot; Dutta, Debasish, "Multi-Direction Slicing for Layered Manufacturing", *Journal of Computing and Information Science in Engineering*, June, 2001, Vol. 1, pp.129-142.
[18] Zhang, J.; Ruan, J.; and Liou, F.W. "Process Planning for a Five-Axis Hybrid Rapid Manufacturing Process", *Proceedings of the Eleventh Annual Solid Freeform Fabrication Symposium*, Austin, TX, pp. 243., August 2000.
[19] Zhang, Jun and Liou, F.W. "Adaptive Slicing for a Five-Axis Laser Aided Manufacturing Process," *Proceedings of the 2001 ASME Design Automation Conference*, Pittsburgh, Pennsylvania, September 9-12, 2001.
[20] O'Rourke, Joseph, "*Computational geometry in C*", 2nd Ed., Cambridge Press, 1998.

[21] Ma, Wan-Chn;Wu, Fu-Che and Ouhyoung Ming, “Skeleton extraction of 3D objects with radial basis function”, *Proceedings of the Shape Modeling International* 2003.
[22] Naf, M.; Szekely, G.; Kikinis, R.; Shenton, M.; Kubler, O., “3D Voronoi Skeletons and Their Usage for the Characterization and Recognition of 3D Organ Shape”, *Computer Vision and Image Understanding* 66, no. 2 (1997): 147.
[23] Sampl, P., “Medial Axis Construction in Three Dimensions and its Application to Mesh Generation”, *Engineering with Computers*, 2001, 17, pp.234-248.
[24] Troulis, M.; Everett, P.; Seldin, E.; Kikinis, R.; Kaban, L.” Development of a three-dimensional treatment planning system based on computed tomographic data”, *International Journal of Oral and Maxillofacial Surgery* 31, no. 4 (2002): 349-357.
[25] Culver, Tim; Keyser, John and Manocha, Dinesh, “Exact computation of the medial axis of a polyhedron”, *Computer Aided Geometric Design*, 21, 2004, pp.65-98.
[26] Dey, Tamal K. and Zhao, Wulue, “Approximate medial axis as a Voroni subcomplex”, *Computer-Aided Design*, 36, 2004, pp.195-202.
[27] Ruan, Jianzhong; Eiamsa-ard, Kunnayut; Zhang, Jun and Liou, F.W., “Automatic Process Planning of A Multi-Axis Hybrid Manufacturing System”, *Proceedings of DETC’02*, September 29—October 2, 2002, Montreal, CANADA.
[28] Picasso M. *et al*, “A simple but realistic model of laser cladding”, *Metallurgical and Materials Transactions*, Volume 25B, April 1994, pp. 281-291.
[29] Ruan, Jianzhong; Eiamsa-ard, Kunnayut; Zhang, Jun and Liou, F.W., “Automatic Multi-axis Slicing Based on Centroidal Axis Computation”, *Proceedings of DETC’05*, 2005, Long Beach, CA, U.S.A.

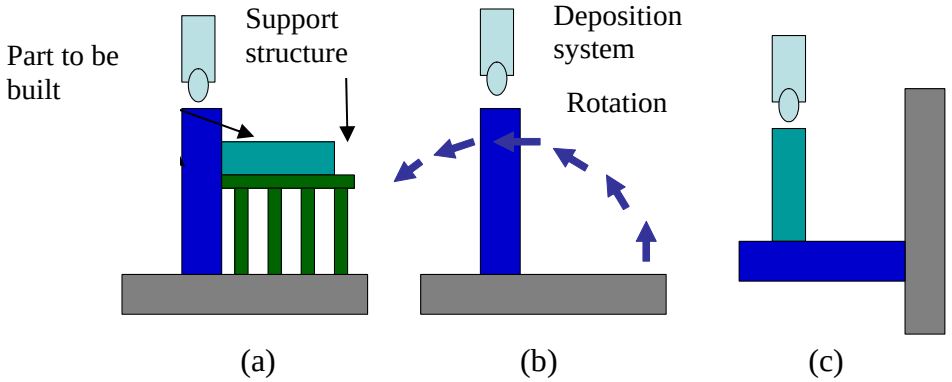

Figure 1. (a) build part with support structure; (b) with multi-axis capability, after building the column, the table can be rotated; (c) After rotation, continue to build the component from another direction

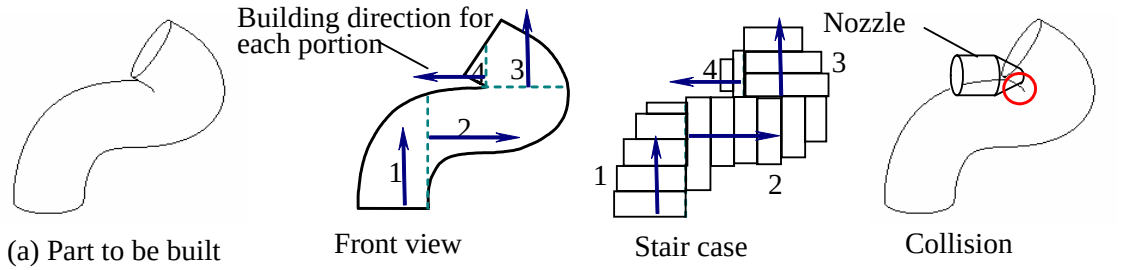

(b) Stair case and collision occurs

Figure 2. A case study to demonstrate limitation of projection-based method

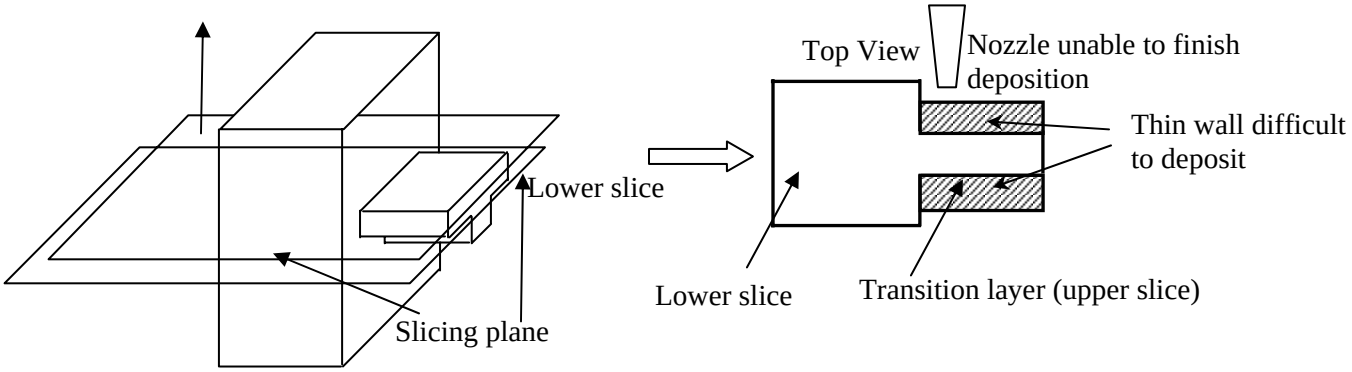

Figure 3. Using transition wall fails to build cylinder overhang

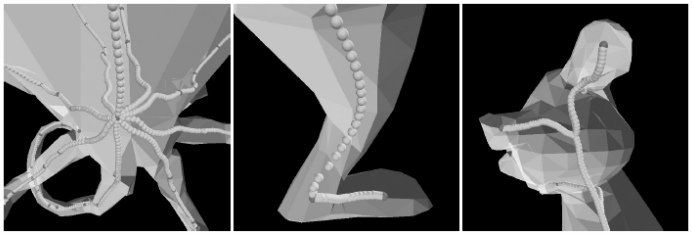

Figure 4. Skeleton of a bunny.

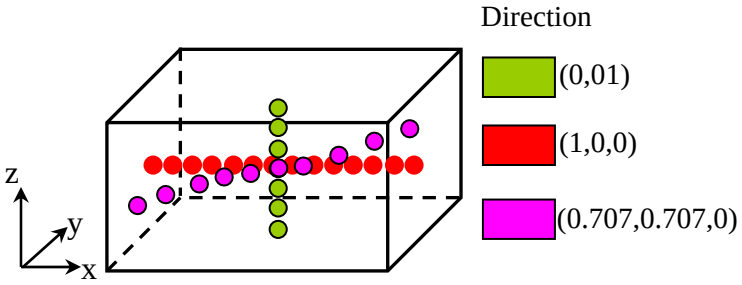

Figure 5. Different centroidal axes

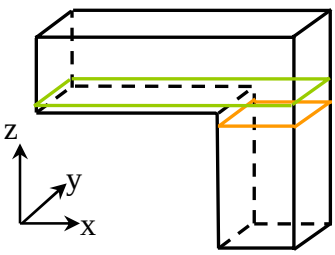

(a) "L" shape geometry

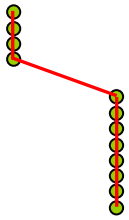

(b) Centrodial axis along "Z" up

Top view

Angle between $\vec{L}$ and {-1,0,0} is 0
Next direction is along X negative

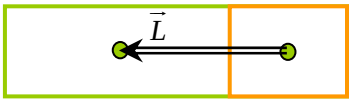

(c) Angle checking

Figure 6. Improper centroidal axis and direction selection

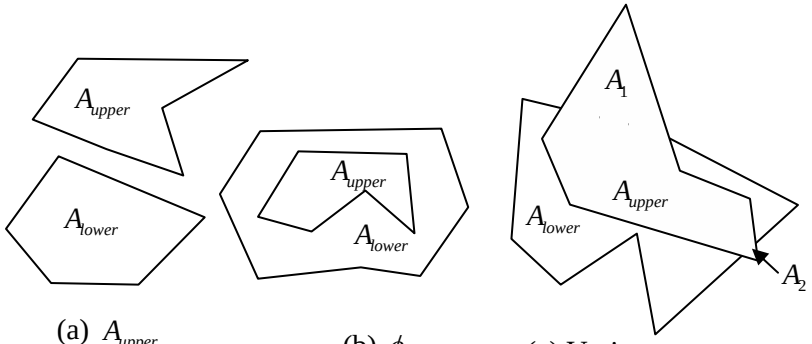

(a) A_{upper} (b) ϕ (c) Various areas

Figure 7. The case of $A_{upper} - (A_{lower} \bigcap A_{upper})$

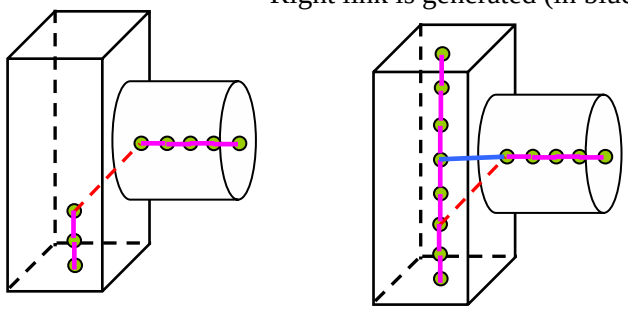

(a) Directly linking two positions yield wrong result (b) Tracking the searching process

Figure 8. Topology link in centroidal axis

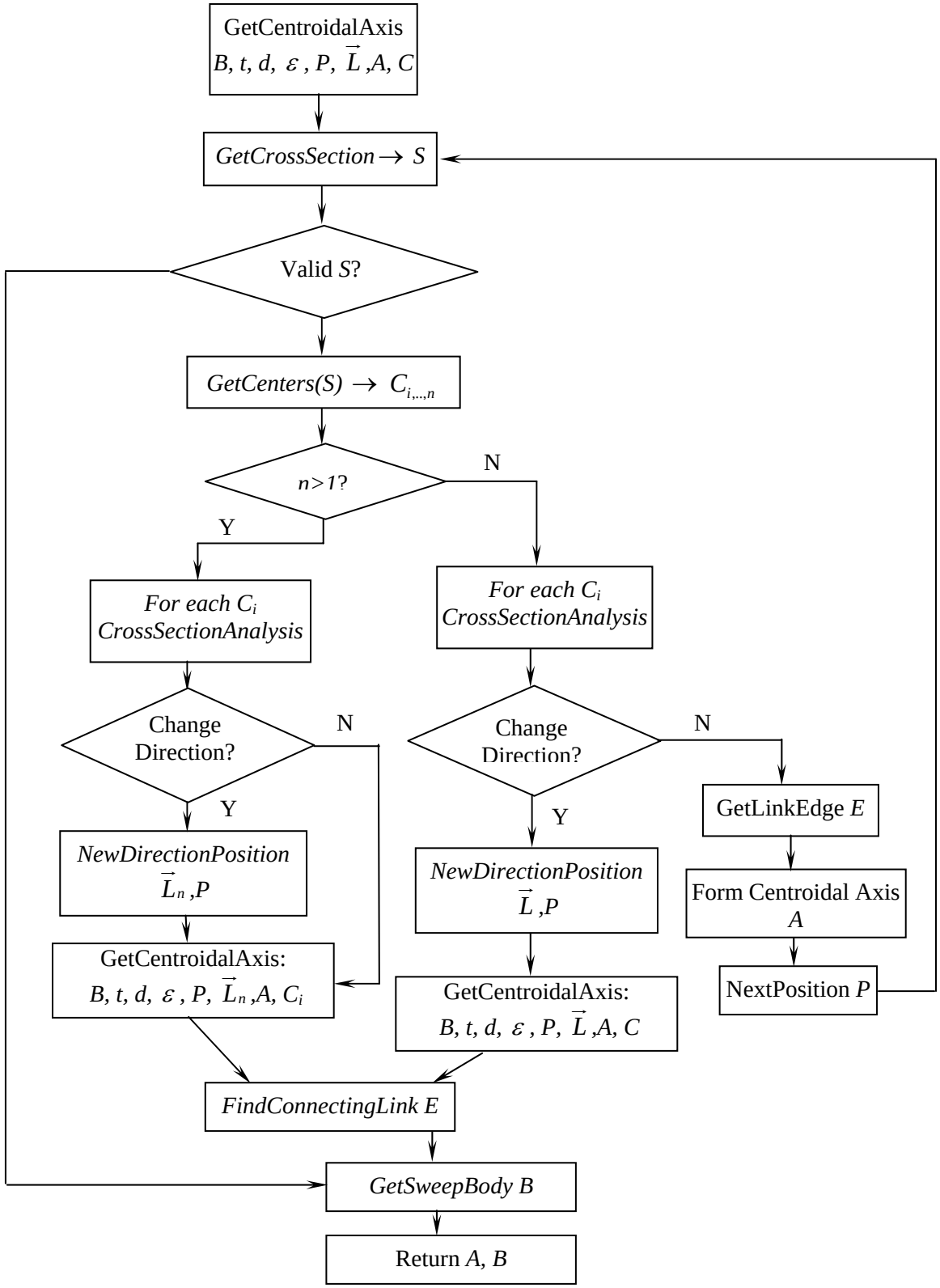

Figure 9. Centroidal Axis Searching Algorithm Chart Flow

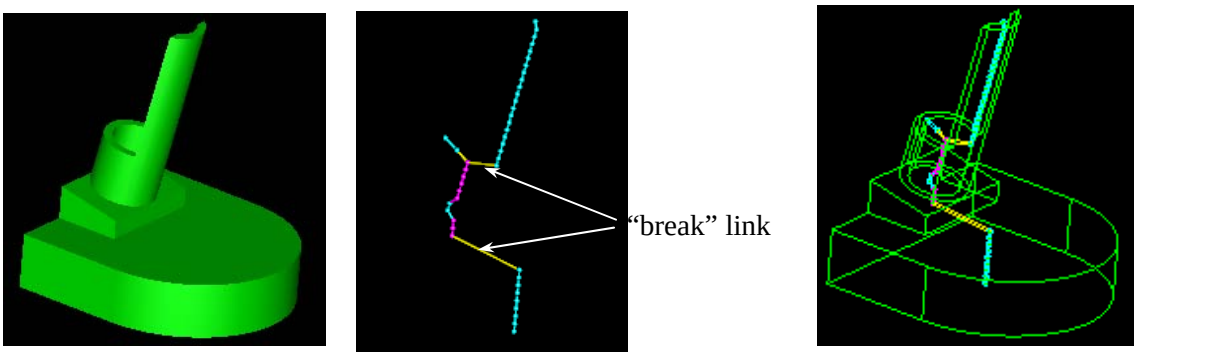

(a) Solid model (b) Centroidal axis (c) Centroidal axis with solid model

Figure 10. Example of centroidal axis extraction

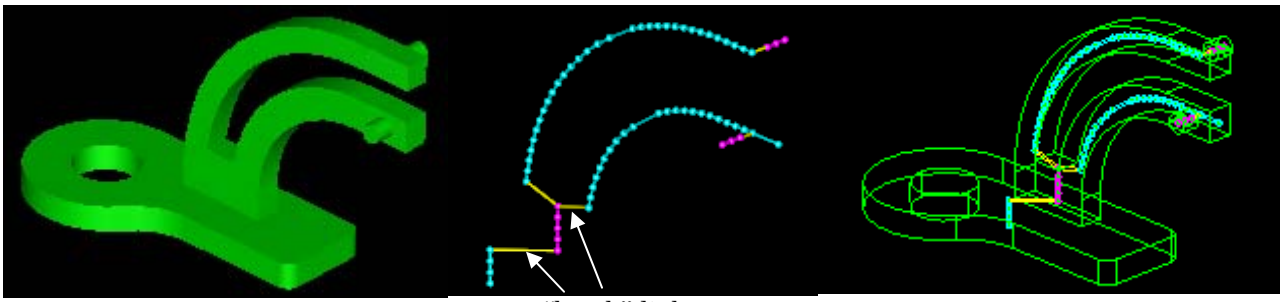

(a) Solid model (b) Centroidal axis (c) Centroidal axis with solid model

Figure 11. Example of centroidal axis extraction

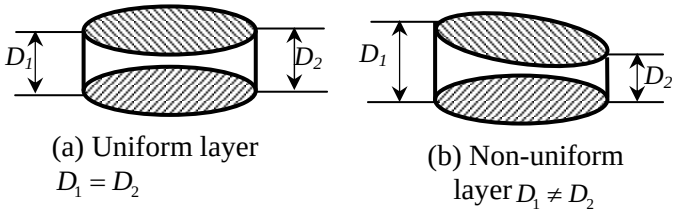

(a) Uniform layer $D_1 = D_2$

(b) Non-uniform layer $D_1 \neq D_2$

Figure 12. Uniform and Non-uniform Layer

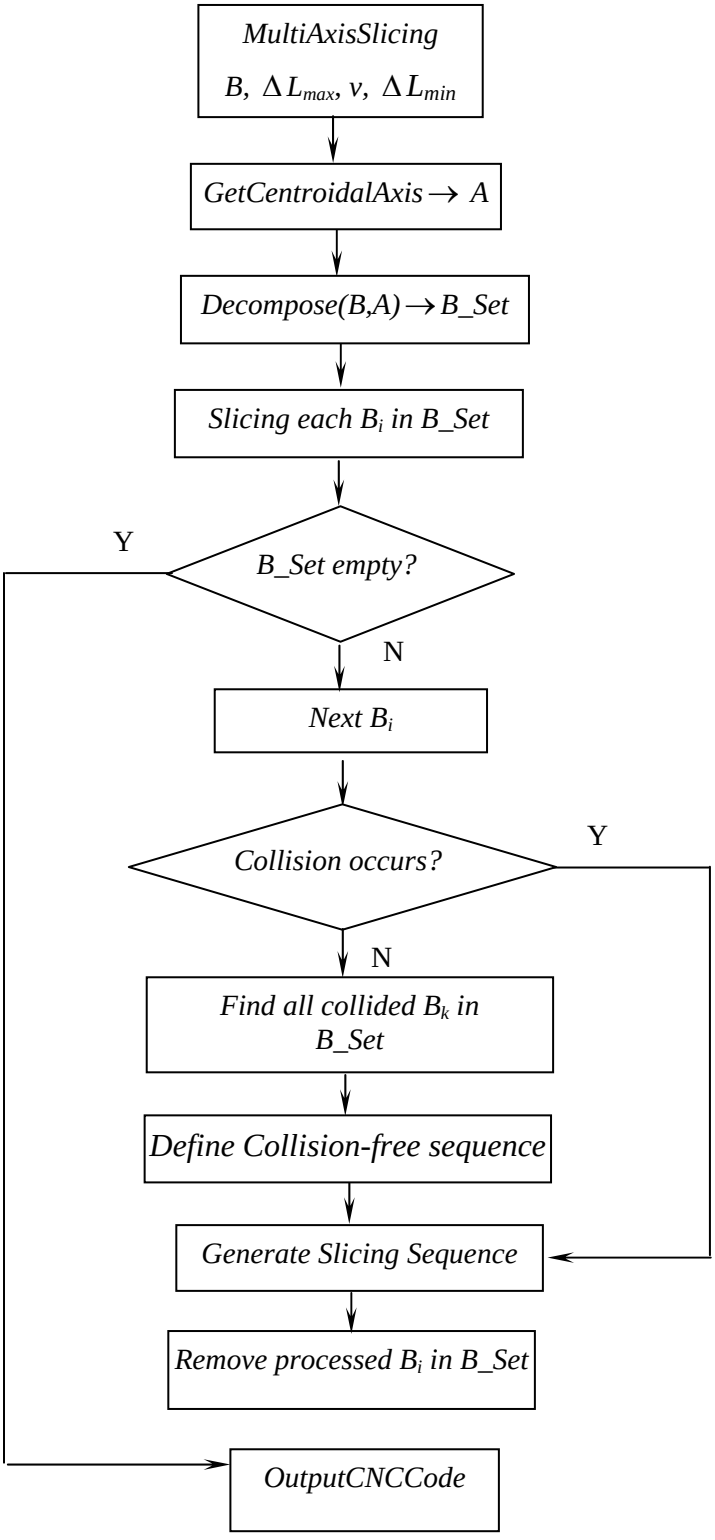

Figure 13. Slicing Algorithm Flow Chart

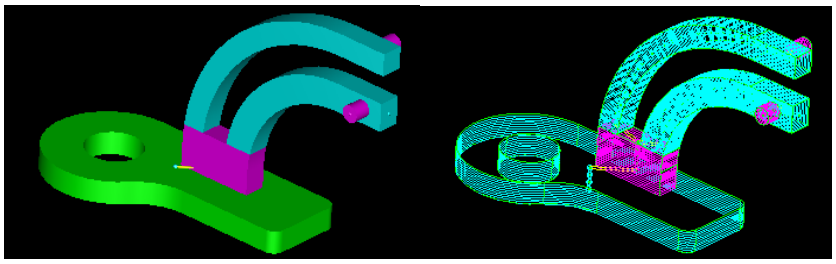

(a) Decomposition result (b) Slicing result

Figure 14. Slicing result of example in Fig. 11

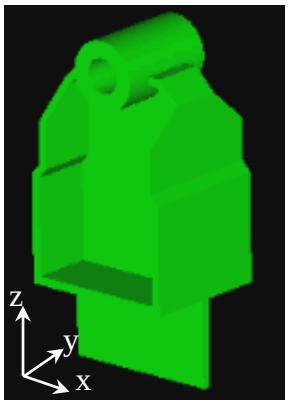

(a) Solid model

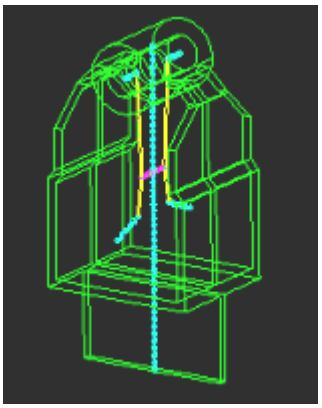

(b) Centroidal axis

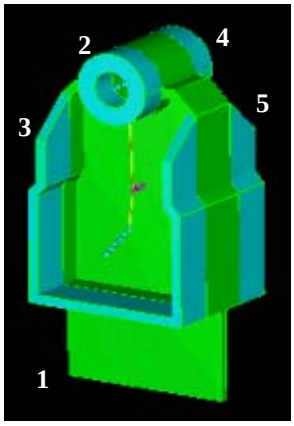

(c) Decomposition result

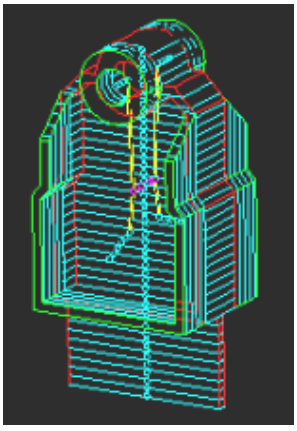

(d) Slicing result

(e) Deposition result after clean out

Figure 15. Hinge example

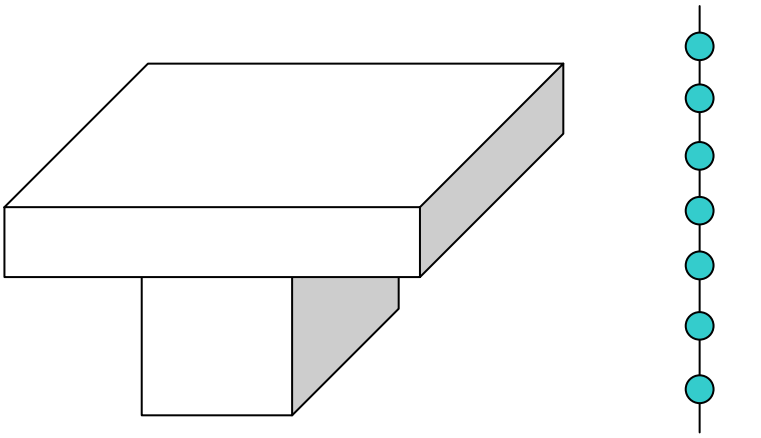

Figure 16. Centroidal axis fails to detect the geometric change

Slicing method	Degree	Control Parameter	Limitation
Cusp height/volumetric difference[10,16]	2.5D	Cusp height/volumetric difference	Only suitable for regular 2.5D system
Projection [17]	Multi-axis	Cusp height	Collision and geometry error
Transition Wall [18]	Multi-axis	Cusp height	Hard to implement on physical machine

Table 1. Slicing Method Summary